Supplementary Information for:

Weakened aerosol-radiation interaction exacerbating ozone pollution in eastern China since China's clean air actions

Hao Yang[1,2], Lei Chen[1], Hong Liao[1], Jia Zhu[1], Wenjie Wang[3], Xin Li[3]

[1]Jiangsu Key Laboratory of Atmospheric Environment Monitoring and Pollution Control, Jiangsu Collaborative Innovation Center of Atmospheric Environment and Equipment Technology, School of Environmental Science and Engineering, Nanjing University of Information Science & Technology, Nanjing 210044, China

[2]College of Materials Science and Engineering, Guizhou Minzu University, Guiyang 550025, China

[3]State Joint Key Laboratory of Environmental Simulation and Pollution Control, College of Environmental Sciences and Engineering, Peking University, Beijing 100871, China

Correspondence to: Lei Chen (chenlei@nuist.edu.cn) and Hong Liao (hongliao@nuist.edu.cn)

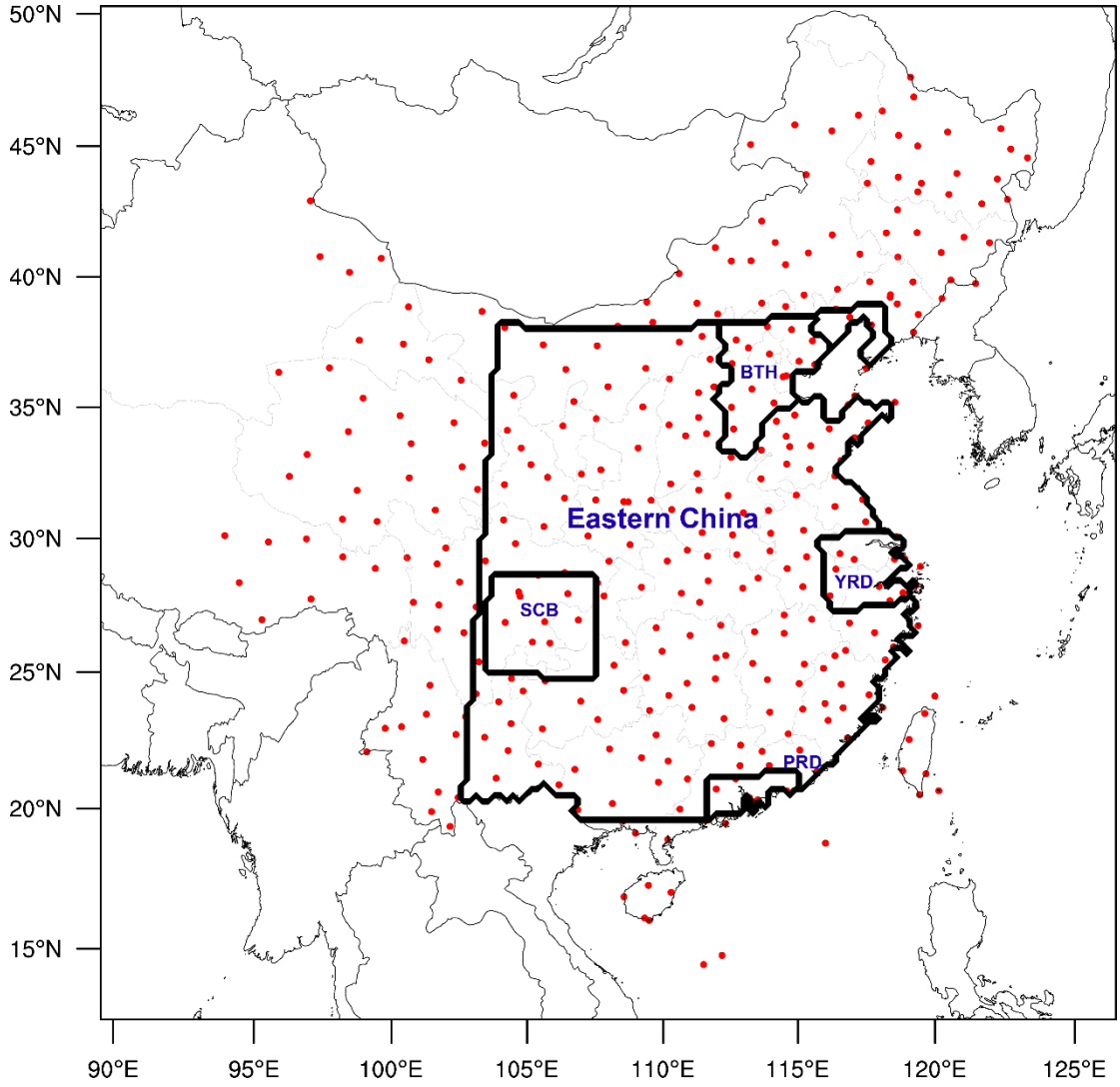

Figure S1. Map of the WRF-Chem simulation domain. Red dots represent meteorological monitoring sites. Five selected regions are also shown in bold black lines, including eastern China, Beijing-Tianjin-Hebei (BTH), Yangtze River Delta (YRD), Pearl River Delta (PRD), and Sichuan Basin (SCB).

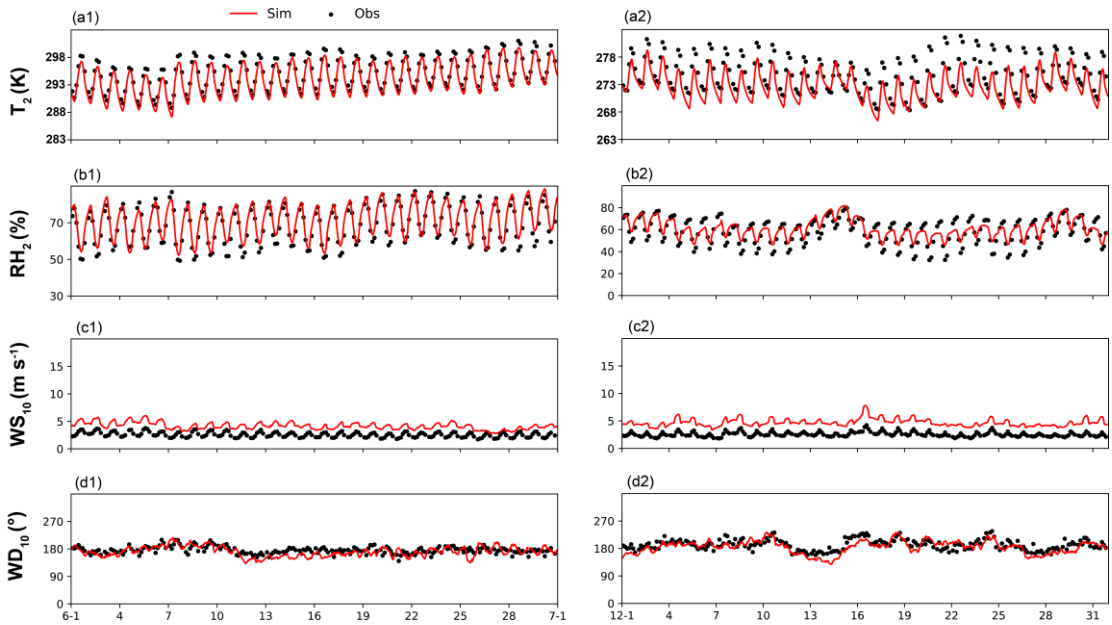

Figure S2. Comparison of 3-hourly observed (black dots) and hourly simulated (red lines) surface meteorological variables of **(a)** 2 m temperature (T_2), **(b)** 2 m relative humidity (RH_2), **(c)** 10 m wind speed (WS_{10}), and **(d)** 10 m wind direction (WD_{10}) averaged over 353 meteorological observation stations during summer (left column) and winter (right column) in 2017.

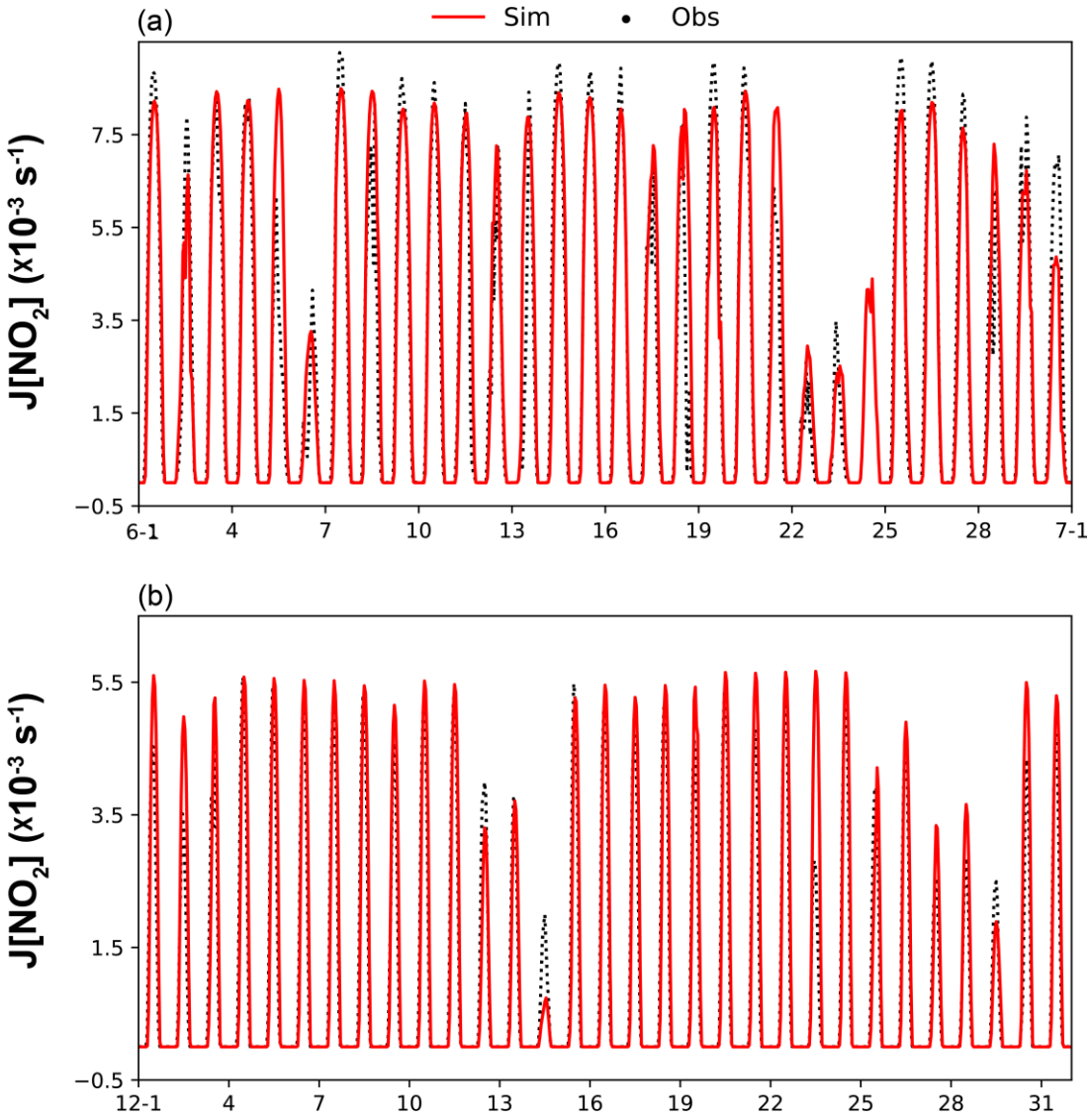

Figure S3. Time series of hourly observed (black dots) and simulated (red lines) surface photolysis rate of NO_2 ($J[NO_2]$) in **(a)** summer and **(b)** winter in 2017.

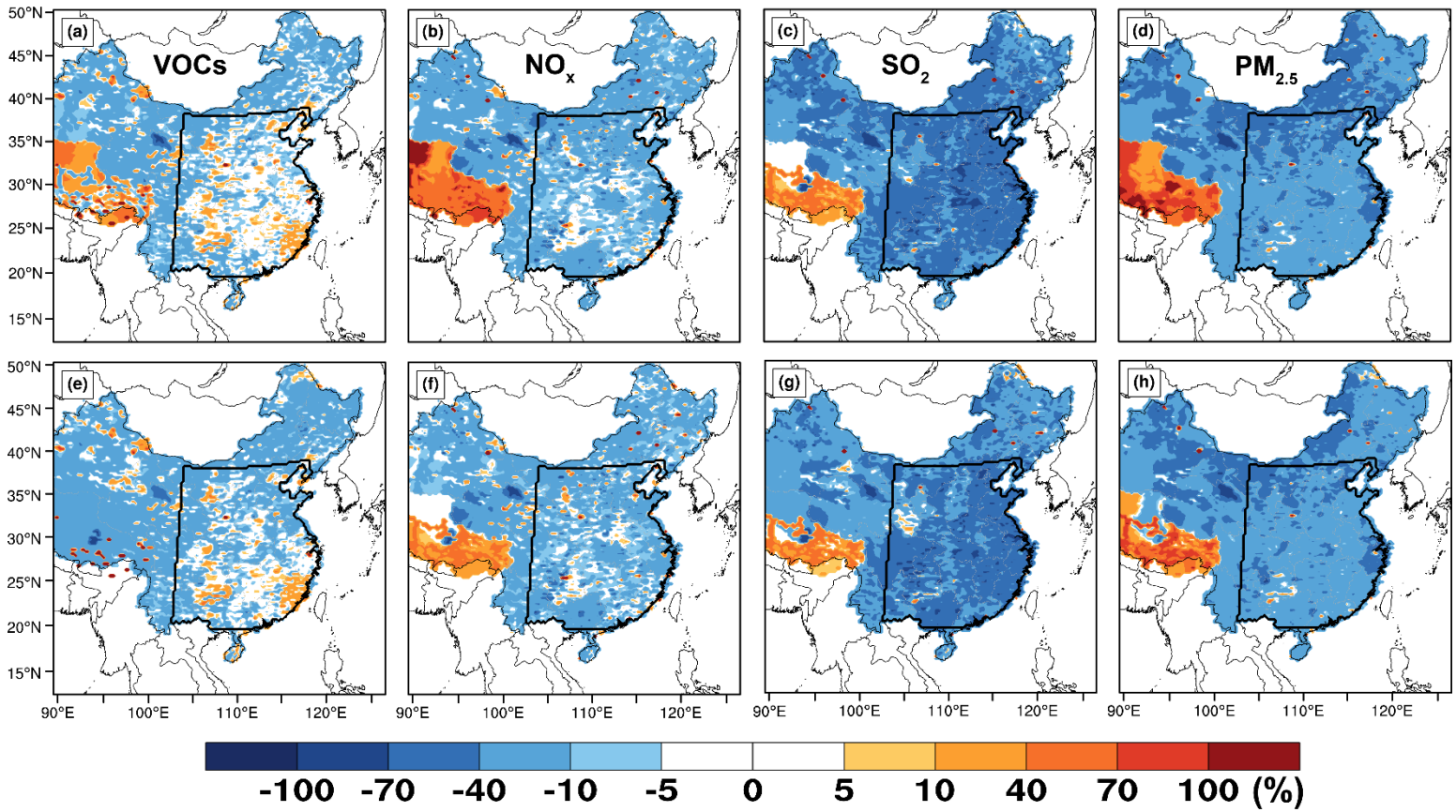

Figure S4. Spatial distributions of changed summer (upper) and winter (bottom) anthropogenic emissions in 2017 relative to that in 2013. **(a, e)** VOCs, **(b, f)** NO_x, **(c, g)** SO_2 and **(c)** $PM_{2.5}$. The enclosed black lines represent eastern China.

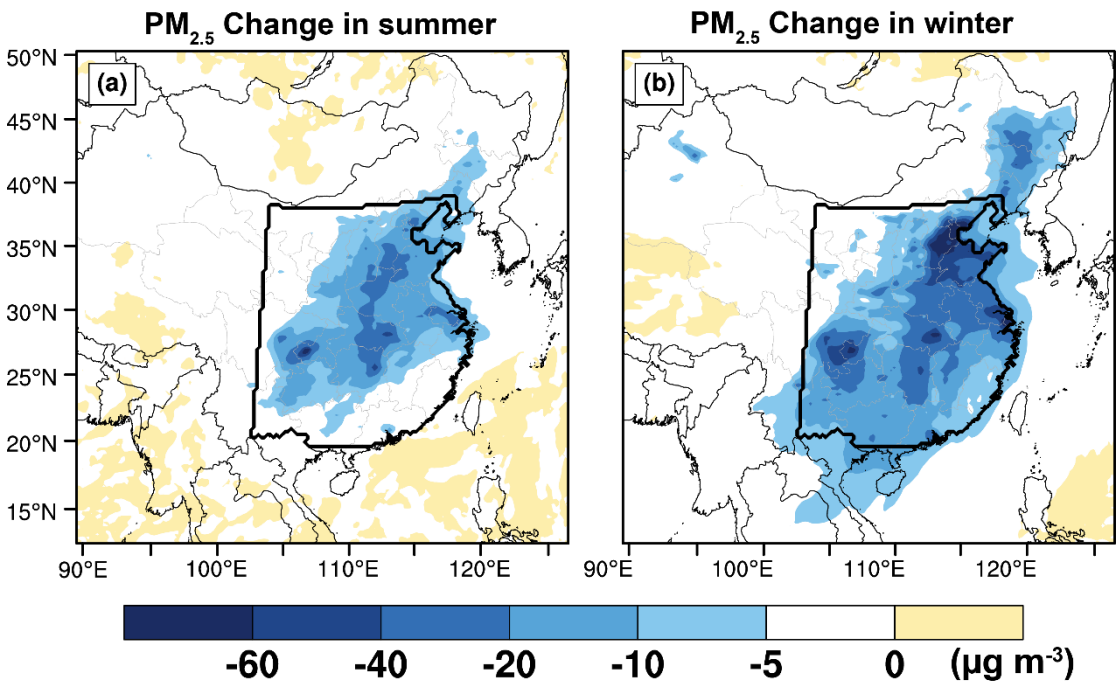

Figure S5. Changes in simulated $PM_{2.5}$ concentrations in **(a)** summer and **(b)** winter from 2013to 2017 due to anthropogenic emission reductions.

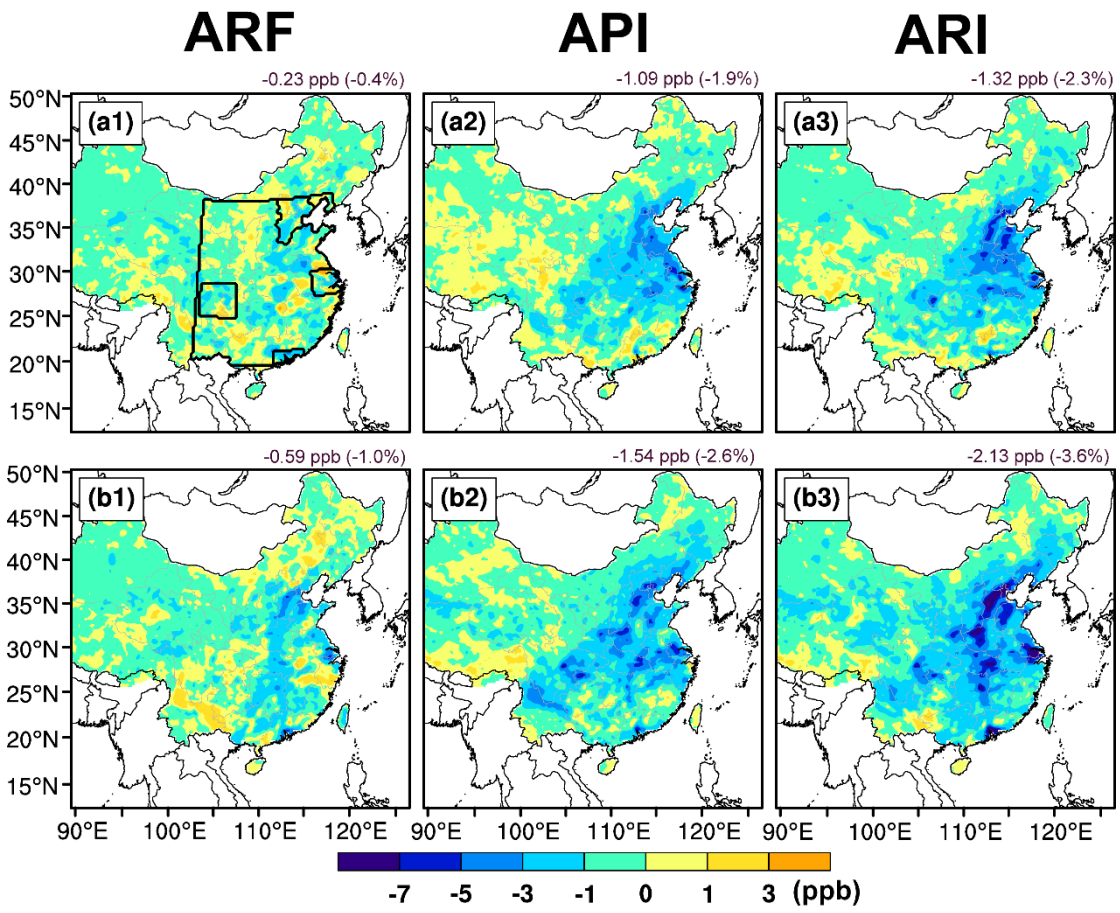

Figure S6. The impacts of **(a1, b1)** aerosol-radiation feedback (ARF), **(a2, b2)** aerosol-photolysis interaction (API), and **(a3, b3)** aerosol-radiation interaction (ARI=ARF+API) on surface-layer MDA8 O_3 in summer under different anthropogenic emission conditions in year 2017 (upper) and year 2013 (bottom).

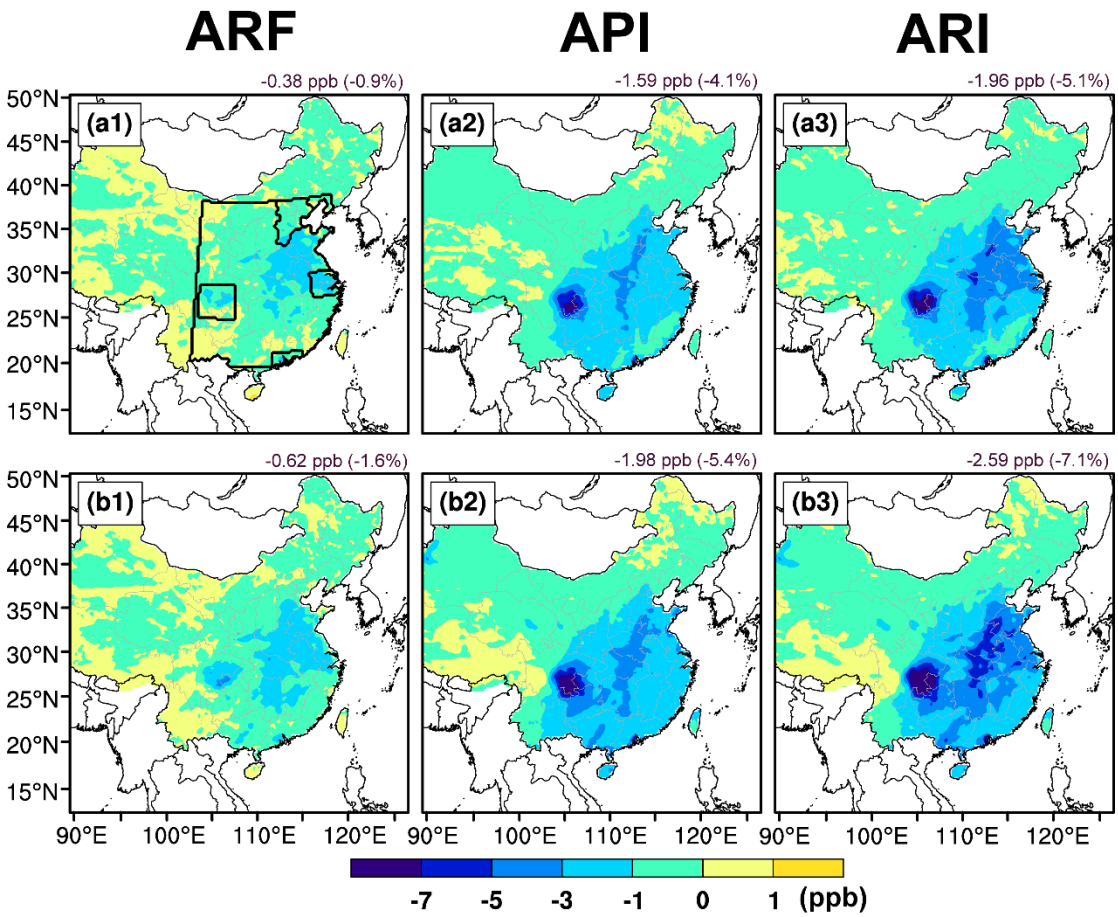

Figure S7. Same as Figure S6 but for winter.

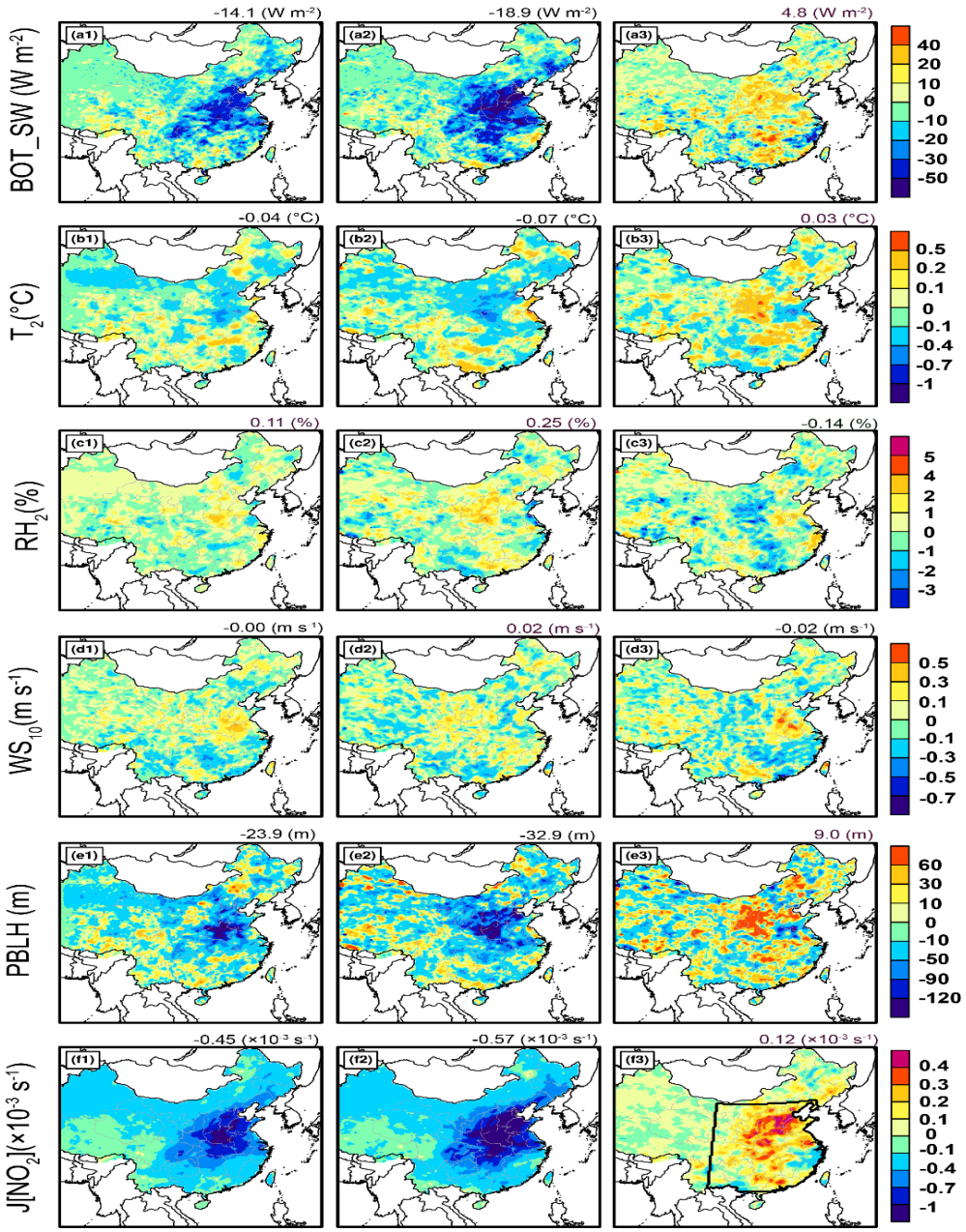

Figure S8. The impacts of aerosol-radiation interaction on **(a)** downward shortwave radiation at the surface (BOT_SW), **(b)** 2-m temperature (T_2), **(c)** 2-m relative humidity (RH_2), **(d)** 10-m wind speed (WS_{10}), **(e)** PBL height (PBLH), and **(f)** J[NO_2] during the daytime (08:00-17:00 LST) in summer. The **(a1-f1)** left panels show the impacts from ΔO_3_ARI_{17E}. The **(a2-f2)** middle panels show the impacts from ΔO_3_ARI_{13E}. The **(a3-f3)** right panels show the impacts from ΔO_3_ΔARI_EMI. Detailed information about ΔO_3_ARI_{17E}, ΔO_3_ARI_{13E}, and ΔO_3_ΔARI_EMI can be found in Figure 1. The enclosed black line in **(f3)** represents eastern China. The mean changes over eastern China are also shown at the top of each panel.

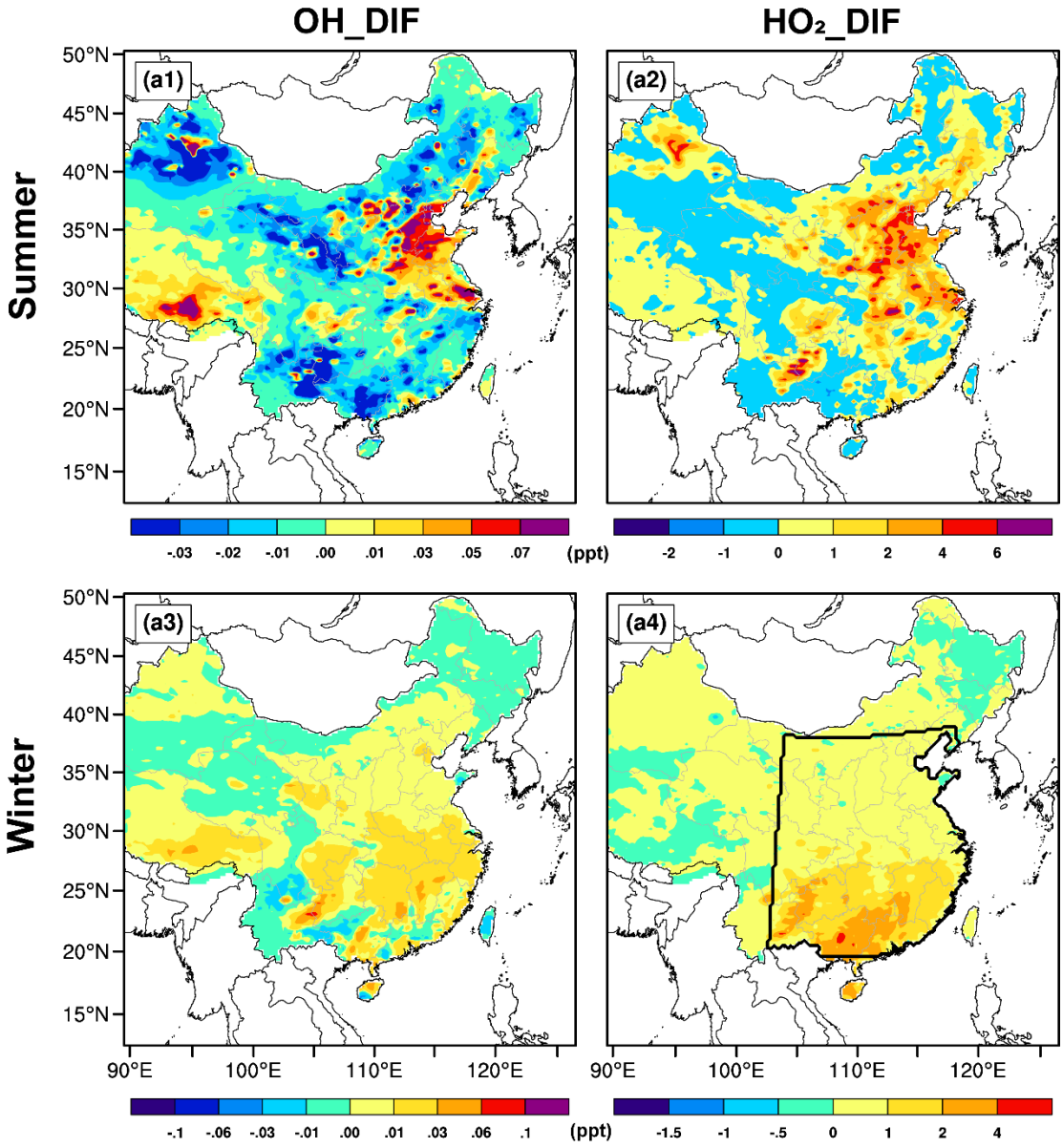

Figure S9. Spatial distribution of changed summer (upper) and winter (bottom) surface-layer **(a1, a3)** OH and **(a2, a4)** HO_2 concentrations from 2013 to 2017 due to anthropogenic emission reductions.